European Journal of Applied Sciences – Vol. 12, No. 06
Publication Date: December 25, 2024
DOI:10.14738/aivp.1206.17981.
Araújo, A. M. C. F., Freitas, D. F. S., Souza, Y. C. A., Albitres, G. A. V., Garcia, E. E., Cestari, S. P., Miguel, M. A. L., & Mendes, L. C. (2024). Building and Evaluating A Green and Multifunctional Composite Based on Poly (butylene adipate-coterephthalate) with Zirconium Phosphate and Clove Essential Oil. European Journal of Applied Sciences, Vol - 12(06). 353-375.

Building and Evaluating A Green and Multifunctional Composite Based on Poly (butylene adipate-coterephthalate) with Zirconium Phosphate and Clove Essential Oil

A.M.C.F. Araújo
Universidade Federal do Rio de Janeiro, Instituto de Microbiologia Paulo de Góes, Centro de Ciências da Saúde, Bloco I, Ilha do Fundão, Rio de Janeiro, Brazil

D.F.S. Freitas
Universidade Federal do Rio de Janeiro, Instituto de Macromoléculas Professora Eloisa Mano, Centro de Tecnologia, Bloco J, Ilha do Fundão, Rio de Janeiro, RJ, Brazil

Y.C.A. Souza
Universidade Federal do Rio de Janeiro, Instituto de Macromoléculas Professora Eloisa Mano, Centro de Tecnologia, Bloco J, Ilha do Fundão, Rio de Janeiro, RJ, Brazil

G.A.V. Albitres
Universidade Federal do Rio de Janeiro, Instituto de Macromoléculas Professora Eloisa Mano, Centro de Tecnologia, Bloco J, Ilha do Fundão, Rio de Janeiro, RJ, Brazil

E.E. Garcia
Universidade Federal do Rio de Janeiro, Instituto de Macromoléculas Professora Eloisa Mano, Centro de Tecnologia, Bloco J, Ilha do Fundão, Rio de Janeiro, RJ, Brazil

S.P Cestari
Centre for Innovation in Polymer Engineering (PIEP), Universidade do Minho, Campus de Azurém, Edifício 15, 4800-058 Guimarães - Portugal

M.A.L. Miguel
Universidade Federal do Rio de Janeiro, Instituto de Microbiologia Paulo de Góes, Centro de Ciências da Saúde, Bloco I, Ilha do Fundão, Rio de Janeiro, Brazil

L.C. Mendes
Universidade Federal do Rio de Janeiro, Instituto de Macromoléculas Professora Eloisa Mano, Centro de Tecnologia, Bloco J, Ilha do Fundão, Rio de Janeiro, RJ, Brazil

ABSTRACT

Although poly(butylene-adipate-terephthalate) (PBAT) is derived from fossil sources, it is classified as a biodegradable polymer because of its predominantly aliphatic ester structure. Synthetic Zirconium phosphate (ZrP) has been widely studied for its notable properties in various fields of human activity. Clove oil (CO) is an eco-friendly material with notable antioxidant and antimicrobial properties. In this context, the present study aimed to develop a green and multifunctional composite based on PBAT incorporated with ZrP, modified ZrP, and CO. The wide-angle X-ray diffraction revealed that the presence of CO promoted the delamination of the phosphates. The thermogravimetric analysis indicated that ZrP and modified ZrP slightly improved the thermal stability of PBAT. The calorimetric evaluations revealed that both ZrP and modified ZrP acted as heterogeneous nucleating agents, increasing the degree of crystallization of PBAT by approximately 70–85%. The incorporation of phosphates and clove oil enhanced the hydrophobicity of the composite films by 20–50%. The thermomechanical analysis indicated a reduction in the glass transition temperature of PBAT and an increase in its linear coefficient of thermal expansion. The type of phosphate and the amount of clove oil influenced the polymer's molecular relaxation behavior. Antimicrobial testing confirmed that the composite effectively inhibited the growth of Gram-positive bacteria (*Staphylococcus aureus* and *Bacillus cereus)* ands the yeast *Candida albicans.*

Keywords: PBAT, zirconium phosphate, clove oil, thermal and surface properties, microbial barrier.

INTRODUCTION

In contemporary society, the reliance on petroleum-derived polymers has grown substantially. However, the use of these polymers presents significant challenges due to the finite nature of oil and gas resources, environmental concerns regarding their degradation, and the risk of cross-contamination during recycling processes. To reduce dependence on petroleum-based polymers, there has been a gradual shift toward replacing non-biodegradable polymers, commonly used in engineering applications, with environmentally friendly, biodegradable alternatives. [1-2] In the context of biodegradable products, one promising application is the replacement of petroleum-based polymers with antimicrobial packaging. However, developing such materials poses a significant challenge in the food safety and shelf-life extension market. This difficulty arises from the broad range of microbial pathogens that can contaminate food and cause illness upon consumption.

Antimicrobial packaging systems play a crucial role in mitigating this risk. Various methods are available for incorporating antimicrobial activity into polymeric materials. These methods include directly integrating antimicrobial agents into the polymers, applying antimicrobial coatings to polymer surfaces, immobilizing antimicrobials through chemical grafting, or using polymers with intrinsic antimicrobial properties. [3] The synthetic aliphatic-aromatic copolyester poly (butylene adipate-co-terephthalate) (PBAT) is derived from fossil fuel-based resources and exhibits biodegradability due to the specific functional groups in its structure. The aliphatic component contributes to its biodegradability, while the aromatic segment imparts superior mechanical properties compared to other biodegradable polymers. [4] These functional groups allow PBAT to be broken down by bacteria under

specific conditions. PBAT exhibits remarkable properties, including high elongation at break and exceptional flexibility, surpassing those of many other biodegradable polyesters. Notably, these characteristics are comparable to those of low-density polyethylene (LDPE). Consequently, PBAT shows significant promise as a biodegradable material. Its versatility allows for applications in various fields, including packaging materials, hygiene products, and biomedical applications. However, it is essential to acknowledge that PBAT's mechanical properties are inferior to those of conventional plastics, which somewhat limits its broader utilization. [1,2,5] Clove oil, extracted through the distillation of the flowers, stems, and leaves of the clove tree, serves as a widely recognized flavoring agent. It contains a multitude of components, many of which display varying levels of antioxidant activity. Notably, eugenol (4-allyl-2methoxyphenol) constitutes 90–95% of clove oil's composition. [6] Numerous scientific reports indicate that clove oil and its primary active compound, eugenol, exhibit beneficial effects on Gram-negative bacteria such as *Escherichia coli, Salmonella*, and *Pseudomonas aeruginosa*, as well as Gram-positive bacteria including *Staphylococcus, Streptococcus*, and *Listeria*. These effects are attributed to the inhibition of bacterial migration, adhesion, virulence factor expression, and biofilm formation. [7] Over time, the antimicrobial activity of essential oils diminishes due to their volatile nature. They are likewise prone to instability, reacting sensitively to oxygen, light, and heat during processing. To preserve and maintain their antimicrobial effects, encapsulating these oils within a delivery system is essential. Researchers have been exploring inorganic carriers as a means to load essential oils. [8-9] Active packaging is an emerging application of biodegradable polymers, offering the potential to enhance antimicrobial activity in films and showing promise over time in industries ranging from biomedical to food packaging. In a study by Morelli and collaborators, natural oil extracted from *Copaifera multijuga* was incorporated into poly (lactic acid) (PLA). The resulting films demonstrated antibacterial properties against *Bacillus subtilis*. The authors concluded that these films show promise as biodegradable active packaging. [10] The investigation of polymer nanocomposites has gained widespread prominence in both academic and industrial domains. In this context, nanoparticles play a pivotal role in meeting both short-term and long-term requirements. Their well-defined structure, size, stability, and uniform dispersion within the polymeric matrix significantly enhance material properties and overall performance. Consequently, the synergistic interaction between the polymer and the filler results in novel hybrid materials with advanced capabilities. Numerous studies have focused on the preparation of PBAT/organoclay nanocomposites. While most aim to optimize the properties of these systems by adding small load content, significant enhancements in nanocomposite properties are achieved only when strong interactions occur between the polymer chains and the silicate lamellae. These improvements depend on both the dispersion state of the organoclays within the polymer matrix and the specific nature and composition of the organoclay used [11]. Many authors have evaluated bioactive nanocomposites using silver nanofillers, which act by inactivating the deoxyribonucleic acid (DNA) of microorganisms [12]. Films with layered nanofillers for food packaging have also been studied for their barrier properties, which hinder the pathway of intercalant molecules, promoting prolonged protection and extending shelf life. Venkatesan et al. prepared a composite based on PBAT blends, improving mechanical strength, thermal properties, and antimicrobial activity against *Escherichia coli* using zinc oxide [3]. The same authors studied the intercalation of montmorillonite with octadecylamine and incorporated it into the PBAT matrix. The antimicrobial evaluation

showed effectiveness against both gram-positive and gram-negative bacteria. Additionally, the films exhibited high mechanical strength and gas barrier properties [13]. For decades, transition metal phosphates, notably zirconium (Zr) and titanium (Ti), have gained increasing importance across various sectors. They can be synthesized through different routes, resulting in nanometric materials with structural similarities to phyllosilicates. Crystalline zirconium phosphate (ZrP) is a lamellar solid acid with notable properties, such as ion exchange capacity, ionic conductivity, and catalytic activity. Its structure consists of overlapping layers of zirconium atoms bonded to oxygen and phosphate groups, making it an alternative to lamellar montmorillonite in the field of polymeric nanocomposites. The P–O-H acid groups can undergo Brønsted acidbase reactions with amines or other molecules, leading to an increase in lamellar spacing and the creation of a new chemical environment, which enhances interaction with various polymeric matrices [14-15]. This work aimed to produce an eco-friendly, multifunctional composite based on PBAT by incorporating zirconium phosphate nanoparticles and clove oil, with potential applications in the food packaging sector. Structural, crystallographic, thermal, surface wettability, molecular mobility, and antimicrobial properties were assessed.

EXPERIMENTAL

Materials

The used materials were poly (butylene adipate-terephthalate) (PBAT) (Ecoflex® F Blend C 1200, BASF S.E.), phosphoric acid (H_3PO_4), zirconium (IV) oxide chloride 8-hydrate ($ZrOCl_2.8H_2O$), ethyl alcohol (Sigma-Aldrich Co.), ethylenediamine (Tedia Brazil) and clove oil (CO) (Phytotratha Cosmeticos LTDA).

Synthesis and Modification of Zirconium Phosphate

The synthesis of zirconium phosphate and its intercalation were performed following previously published work on this subject [16]. In brief, zirconium phosphate was synthesized by mixing 12M H_3PO_4 and $ZrOCl_2 \cdot 8H_2O$ in a Zr:P ratio of 18, followed by reflux and stirring at 110°C for 24 hours. Afterward, the ZrP was intercalated with ethylenediamine using an amine:phosphate ratio of 1:1. The modified material was labeled as ZrP/ED.

Composite and Specimen Preparation

Composite films were prepared by dissolving 6 g of PBAT in 20 mL of chloroform at 25°C with stirring. Concurrently, a dispersion of either ZrP or ZrP/ED in chloroform was prepared to achieve a composite with 2 wt.% of ZrP or ZrP/ED. The PBAT solution was then added dropwise to the ZrP dispersion at 25°C with stirring. Films were formed by pouring the solution onto a Petri dish and drying at 25°C. As a reference, a PBAT film was also prepared. For the addition of clove oil (5 and 10 wt.% based on PBAT content), clove oil was added to the phosphate solution, which was mixed with PBAT solution then poured onto a Petri dish and dried to form a film. The samples were labeled as PBAT, PBAT/ZrP, PBAT/ZrP/ED, PBAT/ZrP/CO_5, PBAT/ZrP/ED/CO_5, and PBAT/ZrP/ED/CO_{10}. A schematic representation of the synthesis, intercalation, and composite preparation of the materials is shown in Figure 1.

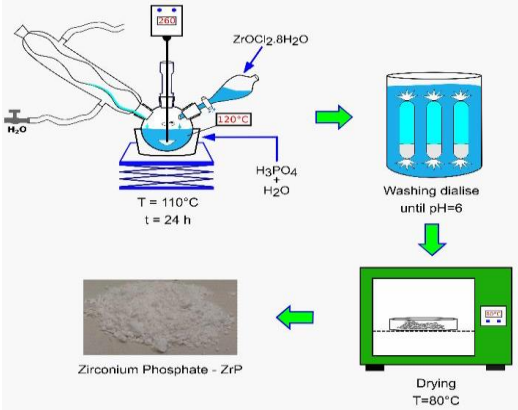

a. ZrP synthesis

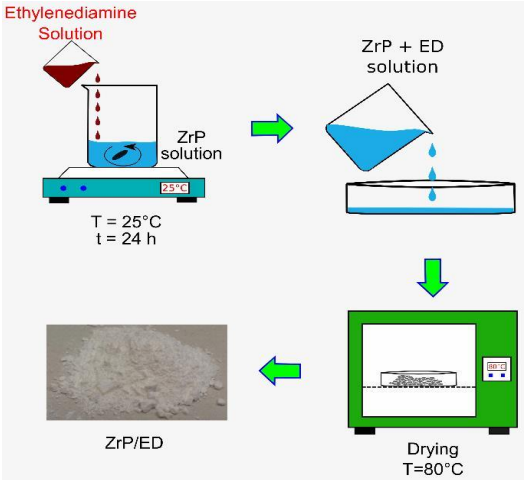

b. ZrP intercalation

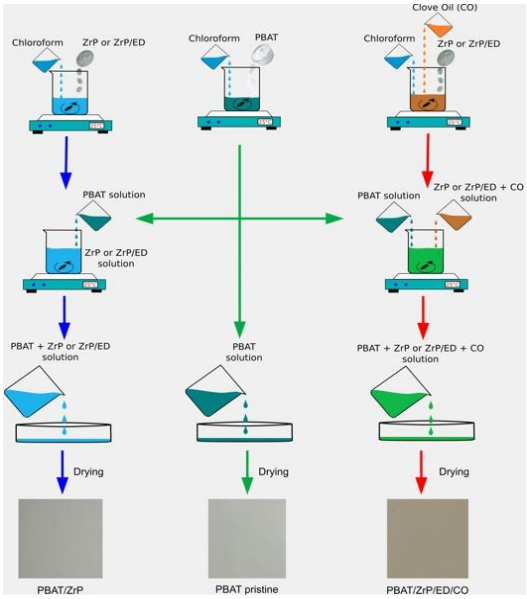

c. Composite preparation

Figure 1: Schematic representation of the ZrP synthesis (a)/intercalation(b) and composites preparation(c)

Fourier Transform Infrared Spectroscopy (FTIR)
Infrared spectroscopy was performed using a Perkin Elmer Frontier model instrument. The spectrum was acquired in ATR mode within the 4000–600 cm^{-1} range, with 60 scans and a resolution of 4 cm^{-1}.

Wide-angle X-ray Diffraction (WAXD)
The X-ray diffraction pattern was obtained using a Rigaku Ultima IV model with CuKα radiation (1.5418 Å), a Ni filter, 30 kV voltage, and a current of 15 mA. The diffraction angle (2θ) ranged from 2° to 50°, with a resolution of 0.05º. Bragg's angle was recorded.

Thermogravimetry (TG/DTG)
Thermal stability was evaluated using a TA Instruments Q500, heating from 10 to 700°C at a rate of 10°C/min, with nitrogen as the carrier gas. Degradation temperatures, including T_{onset}, T_{max}, T_{50} (50 wt.% mass loss), and residue, were recorded.

Differential Scanning Calorimetry (DSC)
Calorimetric parameters were assessed using a TA Instruments Q1000 model. Five thermal cycles were conducted. In the first cycle, the sample was heated from 15 to 190°C at 10°C/min under a nitrogen atmosphere and held at 190°C for 2 minutes to erase the thermal history. The sample was then cooled to 15°C at the maximum rate of the equipment. A second heating cycle was conducted in the same manner as the first. Following that, a cooling cycle to 15°C was performed at 10°C/min. Finally, a third heating cycle was carried out to 190°C at 10°C/min. Crystallization and melting temperatures (T_c and T_m) were recorded. The degree of crystallinity (X_c) was determined based on the ratio of the experimental melting enthalpy to the melting enthalpy of 100% crystalline PBAT (114 J/g) [17].

Thermomechanical Analysis (TMA)
Glass transition temperature (T_g) and the linear coefficient of thermal expansion (LCTE) were monitored according to ISO 11359-2:2021 [18] using a TMA 450 Discovery (TA Instruments). A macro extension probe with 0.2 N was applied, within a temperature range of -50 to 0°C, at a heating rate of 10°C/min, under a nitrogen atmosphere.

Contact Angle
Contact angle (θ) was measured using an OCA15EC – Dataphysics Instruments system to determine the water contact angle on the sample using the YoungLaplace method. A 6 µL drop of water was placed on the film surface with a precision syringe, with automatic temperature drift compensation, and stable, homogeneous illumination of the sample was ensured. The test was conducted in triplicate at room temperature, with consistent light settings. The angle was recorded with the aid of the coupled filming apparatus and software, dpiMA.

Time Domain Hydrogen Nuclear Magnetic Resonance (TDHNMR)
Time-domain hydrogen nuclear magnetic resonance (1H NMR) was conducted using a MARAN Ultra 0.54 T system (23.4 MHz for 1H) from Oxford Instruments, equipped with an 18 mm probe. All data were collected at 30°C, and the 90° pulse length was automatically

calibrated to 7.5 μs. The longitudinal relaxation time (T_1H) was determined from the relaxation curve.

Antimicrobial Activity

Antimicrobial activity was evaluated using the agar diffusion method against the following bacteria: *E. coli* (ATCC 11229), *Salmonella Enteritidis* (13076), *Pseudomonas aeruginosa* (15442), *Staphylococcus aureus* (29213), *Bacillus cereus* (14579), and *Listeria monocytogenes* (19117). The yeast *Candida albicans* (10231) was also tested. The microorganisms were stored at 4°C and activated by cultivation in Tryptic Soy Broth (TSB) at 37°C for 24 hours (for bacteria) and Sabouraud broth at 37°C for 48 hours (for yeast). A cell suspension containing 10^8 colony-forming units per milliliter (CFU/ml) was prepared from the microbial growth in a sterile 0.85% (w/v) saline solution. The suspension was inoculated onto the surface of plates containing Tryptic Soy Agar (TSA) for bacteria and Sabouraud agar for yeast using a swab. After inoculation, 6 mm diameter discs of the sample were aseptically placed onto the surface of the plates, which were then incubated at 37°C for 48 hours. PBAT discs without clove oil were used as a negative control. The presence of growth inhibition halos around the discs was considered a positive result.

RESULTS AND DISCUSSION

Fourier Transform Infrared Spectroscopy (FTIR)

Figure 2 presents the spectra of PBAT and composites. Typical absorptions of PBAT were found at 2,956 cm^{-1} (CH_2 asymmetric stretching), 1,710 cm^{-1} (C=O symmetric stretching), 1,504 cm^{-1} (benzene ring stretching), 1,410 cm^{-1} (CH_2 symmetric stretching), 1,268 cm^{-1} (C-O asymmetric stretching), 1,103 cm^{-1} (C-O stretching), 1,018 cm^{-1} (oxygen close to benzene ring), 936 cm^{-1} (C–O stretching) and 727 cm^{-1} (C–H in benzene ring and stretching of methylene group) corroborated by articles of Weng et al [19] and Zhai and collaborators [20]. For PBAT/ZrP, in addition to the absorptions of the polymer matrix, ZrP-specific absorptions were observed at 3,591 and 3,509 cm^{-1} (stretching of hydrogen bonds between P-O-H and H-O-H in the crystalline interlayer), 3,139 cm^{-1} (OH stretching vibration in P-O-H), 1,617 cm^{-1} (deformation of water molecules within the crystal lattice), 1,075, 1,050, and 968 cm^{-1} (P-O vibration in the PO_4^{3-} group), and 594 cm^{-1} (Zr–O bond vibration) [21-22]. For PBAT/ZrP/ED, PBAT absorptions were also observed; however, due to the reaction between the amine groups of ethylenediamine and the P-O-H groups in the ZrP superimposed lamellae, the absorptions at 3,593, 3,509, and 3,139 cm^{-1} disappeared, owing to the formation of P–O-$+H_3N$-CH_2-CH_2-NH_3^+-O–P. Additional absorptions appeared at 2,957, 2,918, and 2,850 cm^{-1} (C-H stretching of ethylenediamine), 1,562 and 1,542 cm^{-1} ($+H_3N$ asymmetric and symmetric angular deformation), 1,470 cm^{-1} (CH_2 group vibration), 1,064 cm^{-1} (stretching of PO_4^{3-}), 957 cm^{-1} (stretching of P-OH), and 720 cm^{-1} (rocking of CH_2 due to ethylenediamine) [15,23]. Following this, a summary of the clove oil infrared absorptions was provided based on several published articles [24,25]. Eugenol, acetyleugenol, and caryophyllene are the main components of clove oil. Absorptions at 3,516 and 3,071 cm^{-1} are associated with O-H and =C-H stretching, respectively. The stretching of the C-H group is observed at 2,936 cm^{-1}. Between 2,000 and 1,500 cm^{-1}, the following absorptions are observed: 1,765 cm^{-1} (C=O symmetric stretching of eugenol acetate), 1,638 cm^{-1} (C=C stretching of the aromatic ring and allyl group), and 1,611 cm^{-1} (C=C stretching of the aromatic ring). In the range of 1,500–1,000 cm^{-1}, absorptions at 1,431 cm^{-1} (CH_2 stretching),

1,366 cm^{-1} (C-H deformation of the CH_3 group), 1,265 cm^{-1} (C-O stretching), 1,210 and 1,100 cm^{-1} (C-O-C asymmetric stretching), and 1,027–1,032 cm^{-1} (C-H in-phase wag) are registered. Below 1,000 cm^{-1}, absorptions at 994 cm^{-1} (stretching of the allyl group), 990 cm^{-1} (C-H out-of-phase vibration), and 816 cm^{-1} (C-H deformation of the aromatic ring) are assigned. Eugenol is the main component of clove oil. It is a phenol in which the aromatic ring is substituted at the 2-position and 4-position by methoxy and propene groups, respectively. Since it is a hydrocarbon containing both aromatic and aliphatic constituents, its infrared absorptions resemble those of PBAT, a polymer with a hybrid aliphatic and aromatic structure. Therefore, the identification of their characteristic absorptions in the composite spectra becomes challenging. The effects of the phosphates and clove oil addition were carefully observed in the spectral ranges of 4,000– 3,000 cm^{-1} and 1,200–800 cm^{-1} (Figure 3). In the range of 4,000–3,000 cm^{-1}, two groups of spectra with similar outlines were observed.

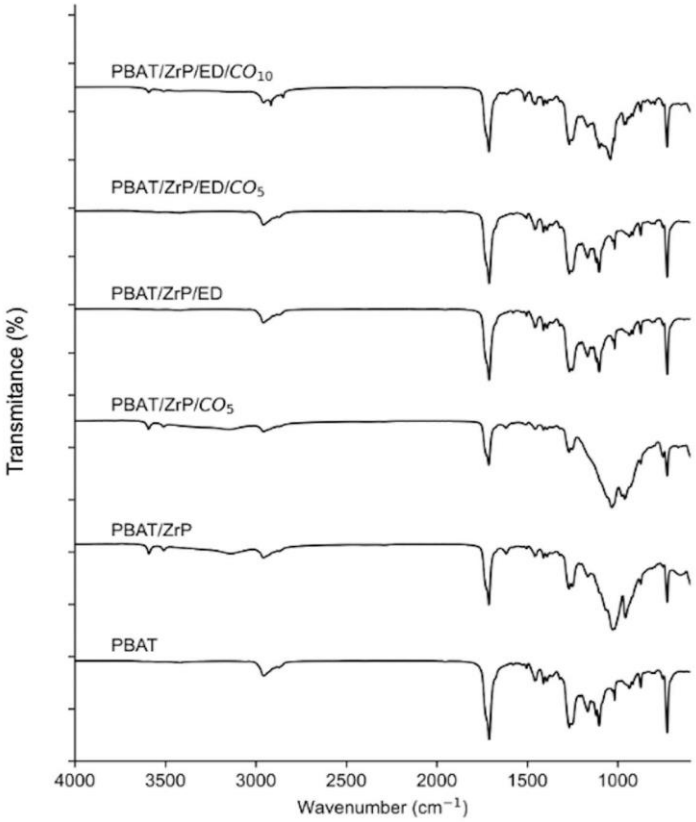

Figure 2: Infrared spectra of the PBAT and composites

One group comprises the samples PBAT/ZrP, PBAT/ZrP/CO_5, and PBAT/ZrP/ED/CO_{10}, while the other includes the samples PBAT, PBAT/ZrP/ED, and PBAT/ZrP/ED/CO_5. In the first group of samples, the ZrP absorptions at 3,593, 3,509, and 3,139 cm^{-1} were highlighted. These absorptions were absent in the second group of samples due to the formation of P–O-+H_3N-CH_2-CH_2-NH_3^+-O–P between adjacent lamellae of ZrP. In the spectral region of 1,200–800 cm^{-1}, the absorptions for the group consisting of PBAT, PBAT/ZrP/ED, and PBAT/ZrP/ED/CO5 overlap, as observed in the other spectral range. For the PBAT/ZrP/CO5 and PBAT/ZrP/ED/CO10 composites, the addition and amount of clove oil influenced the

spectra's outline. This suggests that a change in the crystalline arrangement of the phosphate may have occurred.

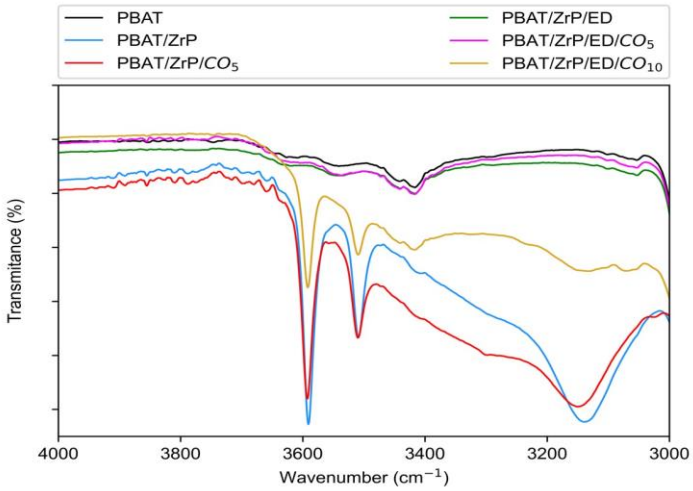

Figure 3: Samples' infrared spectra in the spectral region of 4,000-3,000 and 1,200-800 cm^{-1}

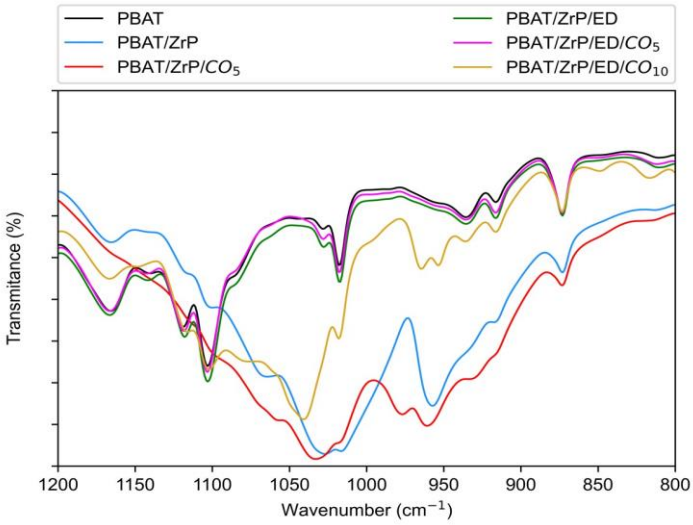

Wide-angle X-ray Diffraction (WAXD)

Figure 4 shows the X-ray diffraction patterns of PBAT and its composites. PBAT exhibited two diffraction angles (2θ) at 14.1° and 16.9°, consistent with the findings of Venkatesan and collaborators [26]. In the PBAT/ZrP composite, the diffraction peaks of PBAT were not observed, likely due to its low crystallization ability. However, the ZrP diffraction peaks at 12.1°, 20.1°, 25.3°, and 34.4°, corresponding to its crystallographic planes d_{002}, d_{110}, d_{112}, and d_{009}, were evident. These results align with those reported by Kang et al. and Jiang *et al.* [27-28]. For the PBAT/ZrP/ED composite, the PBAT diffraction peak around 16° could be considered incipient, while the ZrP peaks at 20.1°, 25.3°, and 34.4° remained. However, the peak at 12.1° shifted to a value lower than 10°. This suggests that some intercalation of ethylenediamine into the ZrP galleries occurred, and the lamellae were partially expanded due to the formation of -P–O^{-+}H$_3$N-CH$_2$-CH$_2$-NH$_3^{+-}$O–P- between adjacent ZrP lamellae. The

presence of clove oil caused significant changes in the composites. For the PBAT/ZrP/CO_5 composite, no ZrP diffraction peaks were detected, which was attributed to its complete delamination by clove oil. The PBAT/ZrP/ED/CO_5 composite appeared similar to its counterpart without clove oil; however, when the clove oil content was increased to 10 wt.%, complete delamination was achieved. Moustafa *et al.* prepared composites based on PBAT incorporated with poly (glycol ethylene) (PEG) as a plasticizer and coffee grounds (CG). X-ray diffraction (XRD) analysis indicated the appearance of a 2θ peak around 18°, which was due to the mutual chemical interaction between the hydroxyl groups of PEG and CG [29]. The results indicated that the structural arrangement of ZrP and ZrP/ED was not affected by the PBAT matrix. Clove oil promoted the breakdown of the crystalline arrangement of both ZrP and ZrP/ED. In the case of PBAT/ZrP/ED/CO_5, it was believed that the amount of clove oil was not sufficient to break the -P–$O^{-+}H_3N$-CH_2-CH_2-NH_3^{+-}O–P- connecting segment between lamellae. Only above 10 wt.%, the eugenol molecules acted as acid catalysts, producing the breakage of that ionic group, leading to the complete delamination of ZrP lamellae. The action of clove oil on the delamination of ZrP and ZrP/ED is schematically depicted in Figure 5. The upper and intermediate lines represent the addition of 5 and 10 wt.% of clove oil for ZrP/ED, while the lower line corresponds to ZrP with 5 wt.% of clove oil. The results are consistent with the infrared analysis.

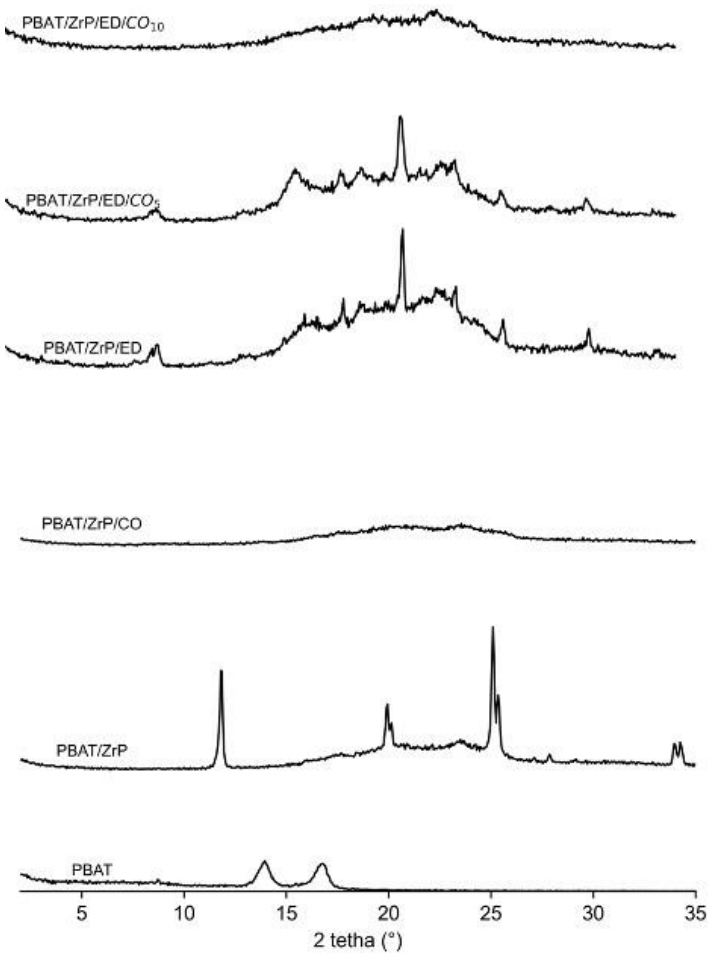

Figure 4: Diffraction patterns of the PBAT and composites

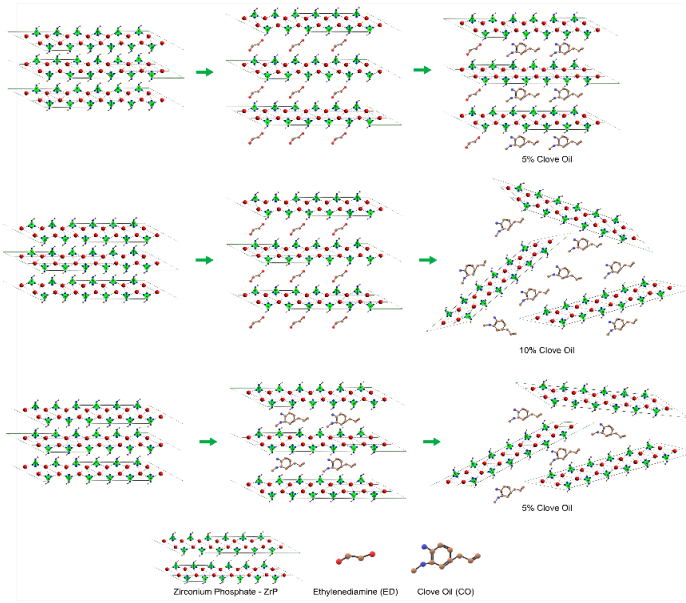

Figure 5: Schematic representation of the ZrP and ZrP/ED delamination by clove oil

Thermogravimetry (TGA)

Figure 6 displays the mass loss and derivative curves. PBAT exhibited only one degradation step. Similarly, the composites PBAT/ZrP and PBAT/ZrP/ED showed a single degradation phase. However, for the composites PBAT/ZrP/CO_5, PBAT/ZrP/ED/CO_5, and PBAT/ZrP/ED/CO_{10}, two degradation steps were detected. The lower stage of decomposition around 110–130°C was attributed to the release of the constituents of clove oil, which have minor thermal stability. Table 1 displays the thermogravimetric data. In general, for the composites, the presence of ZrP or ZrP/ED increased the T_{onset}, but when clove oil was added, T_{onset} was slightly reduced. Similarly, the T_{max} followed the same trend. For PBAT and the composites, all of them degraded 50 wt.% of their mass immediately before reaching T_{max}, suggesting that the PBAT butylene-adipate portion is thermally less stable than its butylene-terephthalate counterpart. Albitres *et al.* investigated the influence of nanocellulose (nCE) on the properties of PBAT. The results indicated that when the nCE content exceeded 1 wt.%, an additional degradation step appeared at a lower temperature, which was attributed to a reduction in PBAT's thermal stability [30]. Venkatesan *et al.* studied composites of PBAT incorporating N, P-doped carbons. Although the authors have stated that the thermal results of the composites matched those of PBAT, the values registered in the article suggested that the addition of N, P-doped carbons improved the PBAT thermal stability [26]. Herein, to some extent, ZrP and/or ZrP/ED acted to slightly increase the thermal stability of the PBAT. Also, the additional degradation step observed after the addition of clove oil does not interfere with its efficiency in the PBAT matrix since the blown films of this polymer are processed between 130-170 °C [31].

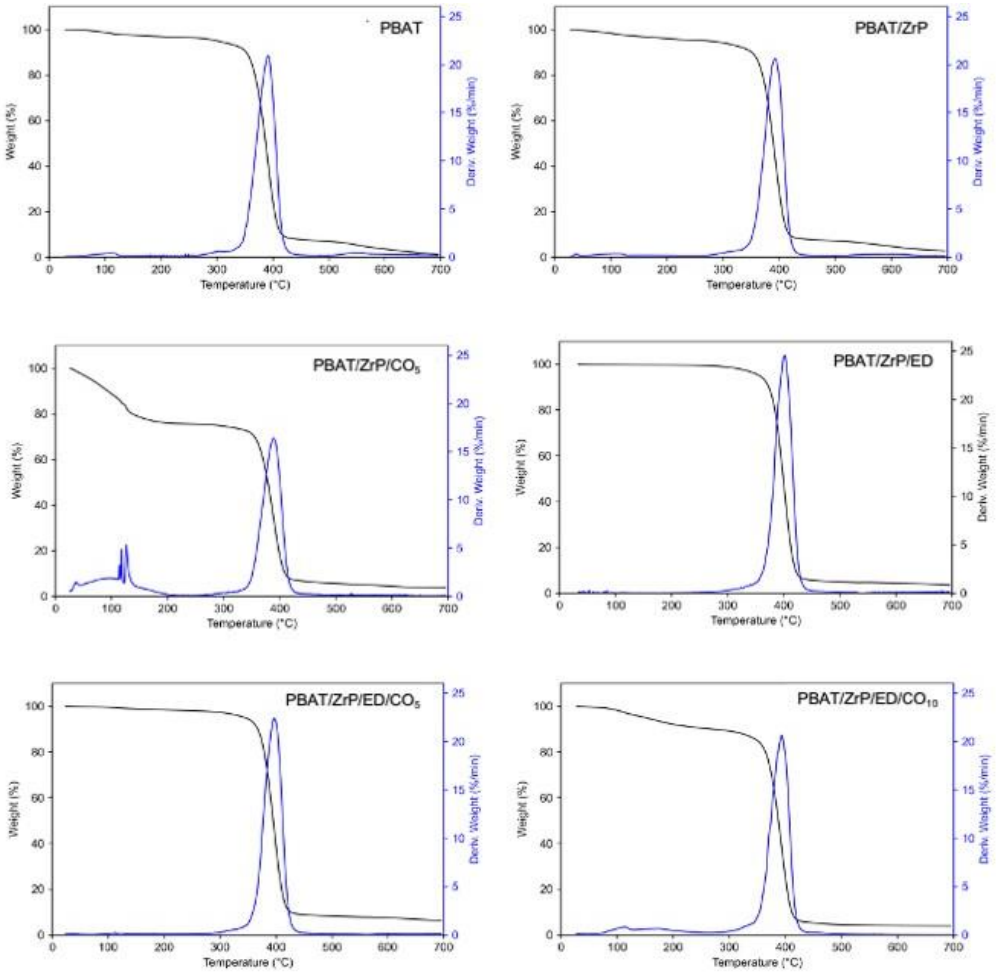

Figure 6: TG and DTG curves of the PBAT and composites

Table 1: Thermogravimetric data of the PBAT and composites

Sample	TONSET (°C)	TMAX (°C)	T_{50} (°C)	Residue (%)
PBAT	364	391	387	1.2
PBAT/ZrP	368	392	389	2.7
PBAT/ZrP/ED	378	402	399	3.5
PBAT/ZrP/CO_5	363	388	378	3.7
PBAT/ZrP/ED/CO_5	374	396	395	6.3
PBAT/ZrP/ED/CO_{10}	369	393	388	4.0

Differential Scanning Calorimetry (DSC)

Figure 7 depicts DSC curves of the first heating, second cooling and last heating, respectively. The first heating curves revealed some interesting features. PBAT presented a single melting peak around 110-135 °C attributed to butylene terephthalate segments as found by Chen and collaborators [32]. The presence of ZrP, ZrP/ED, and clove oil altered the calorimetric curves of the composites. All the curves showed a melting peak at higher temperatures, which made the peak flatter and wider. Additionally, a new peak appeared between 30-50 °C. It was deduced that the phosphates promoted the crystallization of the butylene adipate segments, while clove oil affected the melting process of the butylene terephthalate segments. The

cooling cycles showed opposing effects from the phosphates and clove oil. While the phosphates raised the crystallization temperature (T_c), clove oil lowered it. In the final thermal cycle, it was found that the PBAT's melting temperature was not significantly influenced by the phosphates or clove oil. Table 2 displays the calorimetric data. Clearly, the T_c values shifted to higher temperatures due to the phosphates acting as a heterogeneous nucleating agent. The presence of clove oil eliminated this effect, and it appeared to act as a retardant for PBAT crystallization, particularly in the composites PBAT/ZrP/ED/CO_5 and PBAT/ZrP/ED/CO_5. For each sample, the variation in the crystallization temperature range supported this observation. Regarding the T_m, there was a notable variation in the melting temperature, reflecting an increase in T_m promoted by the phosphates and a decrease induced by clove oil. In all composites, the degree of crystallinity (X_c) increased with the addition of ZrP and ZrP/ED, due to their role as nucleating agents, even in the presence of clove oil. The PBAT/ZrP/ED/CO_{10} composite exhibited the smallest increase in X_c 14%), while for the other composites, the increase in X_c ranged from 70% to 85%. Seligra et al. described a decrease in the melting temperature of PBAT/starch nanoparticles composites, which was attributed to the formation of imperfect crystals in the butylene terephthalate segment [33]. Moustafa et al. pointed out that no significant variation in the melting temperature was observed in composites of PBAT enriched with coffee ground waste as a filler [29]. Costa et al. investigated blends of poly (butylene succinate) (PBS) and PBAT. The authors noted that PBS promoted a slight upward shift in the PBAT melting peak, along with a significant reduction in melting enthalpy and crystallinity. These changes were attributed to the physical interactions between the two polymers [34]. Li et al. investigated the crystallization behavior of PBAT filled with various forms of halloysite: neat, calcined, and organo-modified. The study explored the impact of these fillers on PBAT's crystallization process. Notably, the presence of the filler at 5 and 10 wt.% led to a gradual increase in the crystallization temperature. According to the authors, the filler promoted a heterogeneous nucleation process for PBAT's chains [35]. According to Albitres et al., the planar arrangement of the butylene terephthalate units in the PBAT chain restricts the degree of freedom for chain conformation, thereby enabling its crystallization. Conversely, the butylene adipate portion, composed of 10 aliphatic carbons, possesses a greater degree of freedom, which hinders its crystallization [30]. developed active packaging films based on nanocomposites of PBAT and cellulose nanofibers (CNS, 5 wt.%) encapsulated with eugenol and linalool. The authors observed a slight increase in the degree of crystallinity, which was attributed to the role of the modified nanocellulose as a nucleating agent [36]. It was observed that phosphates and clove oil had conflicting effects on the thermal events of PBAT. As mentioned, the wide degree of freedom of the butylene adipate portion made its crystallization difficult. Although the butylene terephthalate segments have a lower degree of freedom, the copolymeric nature of PBAT still resulted in a low degree of crystallinity. These results are consistent with the FTIR and WAXD analyses.

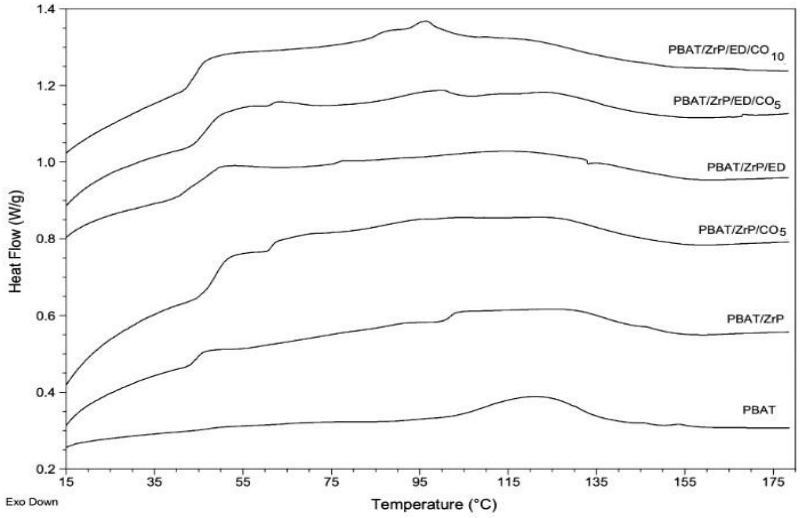

a. First heating cycle

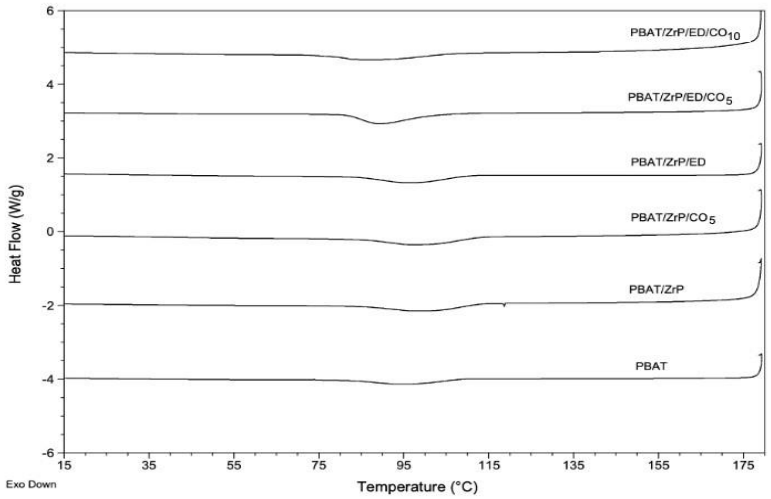

b. Second cooling cycle

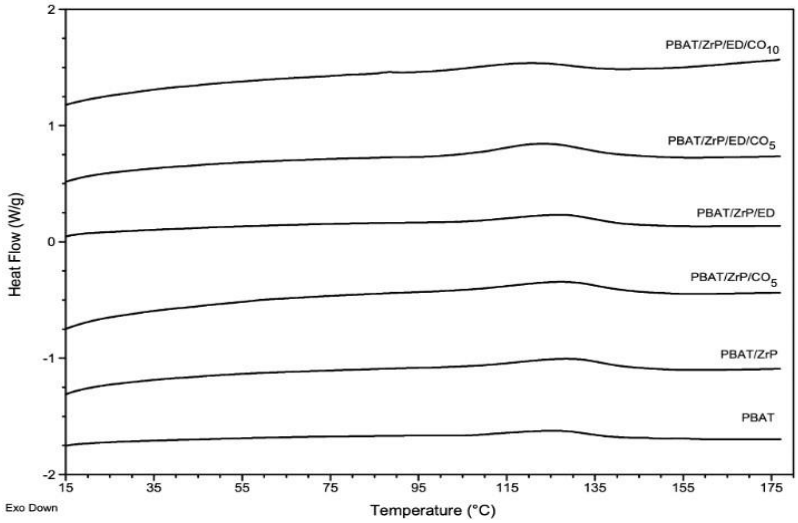

c. Last heating cycle

Figure 7: DSC curves of the samples: a) first heating, b) first or second cooling and c) third heating

Table 2: PBAT and composites' calorimetric data

Sample	T_c (°C)	Onset and final crystallization temperature (°C)	Tm (°C)	Onset and final melting temperature (°C)	ΔH_m (J/g)	X_c (%)
PBAT	94	79-109	126	108-138	7.7	6.8
PBAT/ZrP	101	81-116	129	103-150	13.3	11.9
PBAT/ZrP/ED	97	80-115	128	101-145	12.5	11.2
PBAT/ZrP/CO_5	100	83-115	128	103-142	13.3	11.9
PBAT/ZrP/ED/CO_5	90	79-106	124	101-140	14.2	12.7
PBAT/ZrP/ED/CO_{10}	88	73-105	119	102-138	8.9	7.9

Contact Angle

The sessile drop of water on the film surface is shown in Figure 8. The images revealed that the contact angle varied with the incorporation of ZrP, ZrP/ED, and clove oil. All samples exhibited half-spherical water droplets. Figure 9 presents the contact angles (θH_2O) of PBAT and its composites. PBAT is well known as a hydrophobic polymer, and the θH_2O value aligns with the results reported by Venkatesan and collaborators [26]. The presence of ZrP and ZrP/ED increased the hydrophobicity of PBAT. The degree of repellence increased by approximately 19% and 23% for PBAT/ZrP and PBAT/ZrP/ED, respectively. When clove oil was added to the composites, the PBAT/ZrP/CO composite showed a higher θH_2O value, exhibiting a 49% increase in repellence. The increase in repellence for PBAT/ZrP/ED/CO_5 and PBAT/ZrP/ED/CO_{10} composites was approximately 17% and 26%, respectively. Tavares et al. developed composites by incorporating lignin into the PBAT matrix. According to the authors, the increase in θH_2O was beneficial for applications where the permeation of oxygen and water must be minimized to prevent microbial proliferation [37]. Nanoparticles of titanium dioxide (TiO_2), zinc oxide (ZnO), silicon dioxide (SiO_2) and cardanol oil were incorporated into blends of poly (lactic acid) (PLA)/PBAT. The authors attributed the increase in contact angle to the presence of pores formed by the nanoparticles [38]. Ginger oil and lime peel oil were incorporated into blends of PBAT/PLA. It was observed that in blends with a higher content of PLA, the contact angle decreased, while the opposite behavior was observed in those enriched with PBAT. The increase in hydrophobicity was attributed to the strong interaction between the oils and the presence of both aromatic and aliphatic carbon portions in the PBAT repeat units [39]. There is a study in which an increase in the hydrophobicity of PLA was observed due to the presence of halloysite nanotubes and clove oil [40]. Herein, the presence of both phosphates and clove oil influenced the contact angle. The highest repellence values were found for the composites PBAT/ZrP/CO_5 and PBAT/ZrP/ED/CO_{10}, where a synergistic effect between ZrP and clove oil can be attributed. For the other composites, the effect of the phosphates' hydrophobicity prevailed. These results are consistent with the X-ray diffraction, infrared, and DSC analyses.

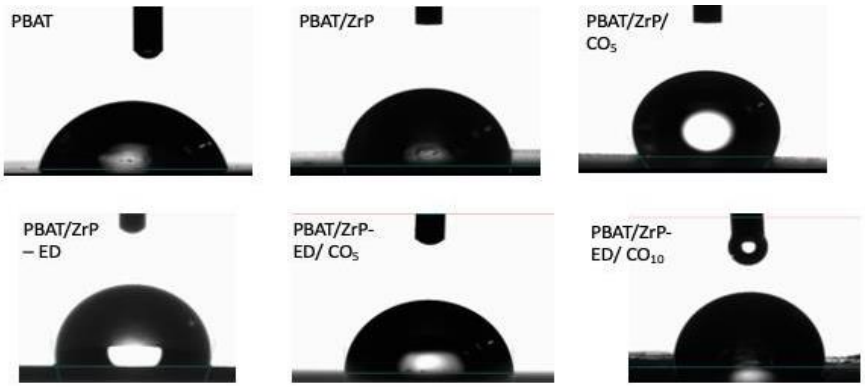

Figure 8: Images from contact angle test of PBAT and composites

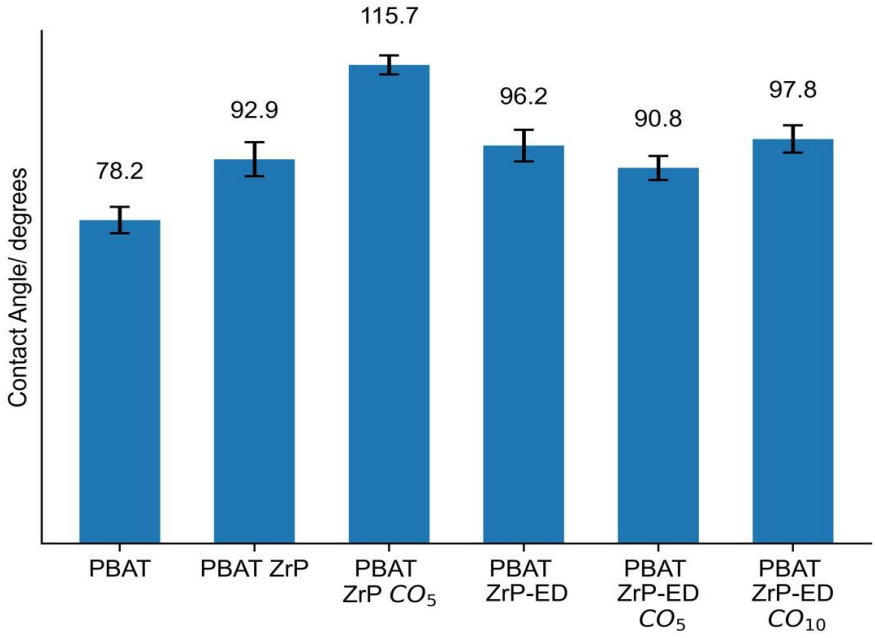

Figure 9: Contact angle value of PBAT and composites

Thermomechanical Analysis (TMA)

Table 3 presents the values of glass transition temperature (T_g) and the linear coefficient of thermal expansion (α, LCTE), before and after T_g. For all composites, a decrease in T_g was observed following the incorporation of phosphates. Generally, the addition of clove oil resulted in an additional reduction in T_g, although this effect appeared to be less pronounced than that of the phosphates. The α values showed no consistent trend. Each composite exhibited a specific α value, independent of the addition of phosphate and/or clove oil. Before and after T_g, the composites exhibited thermal expansion values higher than PBAT alone. Hassan et al. studied the effects of nozzle temperature, infill density, top and bottom solid layer raster angle, and infill pattern as variables for a 3D-printed polymer blend of PBAT, poly(lactic acid) (PLA), and polybutylene succinate (BioPBS). The linear coefficient of thermal expansion varied as a function of each parameter, with the lowest and highest LCTE values being 106.8 and 111.5 µm/m°C, respectively [41]. Josselin and collaborators investigated the linear coefficient of thermal expansion in composites constituted by PBAT and continuous

flax fiber (cFF). For PBAT, the LCTE value was 240 μm/m °C [42]. It is well-established that the coefficient of thermal expansion (LCTE) indicates how quickly or slowly a material expands with temperature. For hybrid materials, the LCTE value depends on the contribution of each component. The higher the coefficient of expansion, the greater the material's thermal expansion with temperature. In this study, both below and above T_g, the presence of phosphates and clove oil promoted an increase in the LCTE. The results suggest that phosphates have a significant influence on LCTE, likely due to their greater thermal conductivity compared to PBAT and clove oil.

Table 3: T_g and LCTE of PBAT and composites

Sample	T_g (°C)	(α) before T_g (μm/m °C)	(α) after T_g (μm/m °C)
PBAT	-33	12.7	204.6
PBAT/ZrP	-37	70.8	235.3
PBAT/ZrP/CO_5	-41	43.5	157.4
PBAT/ZrP/ED	-38	13.9	165.2
PBAT/ZrP/ED/CO_5	-39	---*	---*
PBAT/ZrP/ED/CO_{10}	-40	89.2	235.1

* no determined

Time Domain Hydrogen Nuclear Magnetic Resonance (TDHNMR)

Relaxometry is a technique used to evaluate molecular dynamics through nuclear magnetic moments, which are related to the atomic and molecular motion of a sample. It provides insights into the physical and chemical characteristics of materials. T_1H (spin-lattice relaxation) refers to the longitudinal relaxation time, which involves the return of magnetization to thermal equilibrium. This relaxation process is often represented as distributions in the relaxation domain [43]. Figure 10 presents the domain curves of the T_1H longitudinal relaxation times of the PBAT and composites. For each relaxation peak, T_1H is highlighted. The domain curve of PBAT showed a single relaxation peak around 2×10^4 - 1.25×10^5 ms. For PBAT/ZrP, two relaxation domains were observed: one below 2×10^4 ms and another between 4×10^4 - 8×10^4 ms. PBAT/ZrP/ED exhibited one relaxation domain around 2×10^4 - 1.5×10^5 ms. After the addition of clove oil, the PBAT/ZrP/CO_5 composite exhibited behavior similar to PBAT/ZrP. The PBAT/ZrP/ED/CO_5 composite showed three relaxation peaks: two between 10^4 - 10^5 ms and another above 10^6 ms. PBAT/ZrP/ED/CO_{10} showed two relaxation peaks: one below 10^4 ms and another between 10^4 - 10^5 ms. Albitres et al. studied the effect of adding nanocellulose (nCE) to PBAT. The nCE content had a random effect on the molecular relaxation of PBAT and was considered responsible for the stiffening of the polymer matrix [30]. In general, the molecular mobility of PBAT increased with the presence of phosphates and clove oil. This variation in molecular mobility supports the findings from the FTIR, WAXD, DSC, and contact angle analyses.

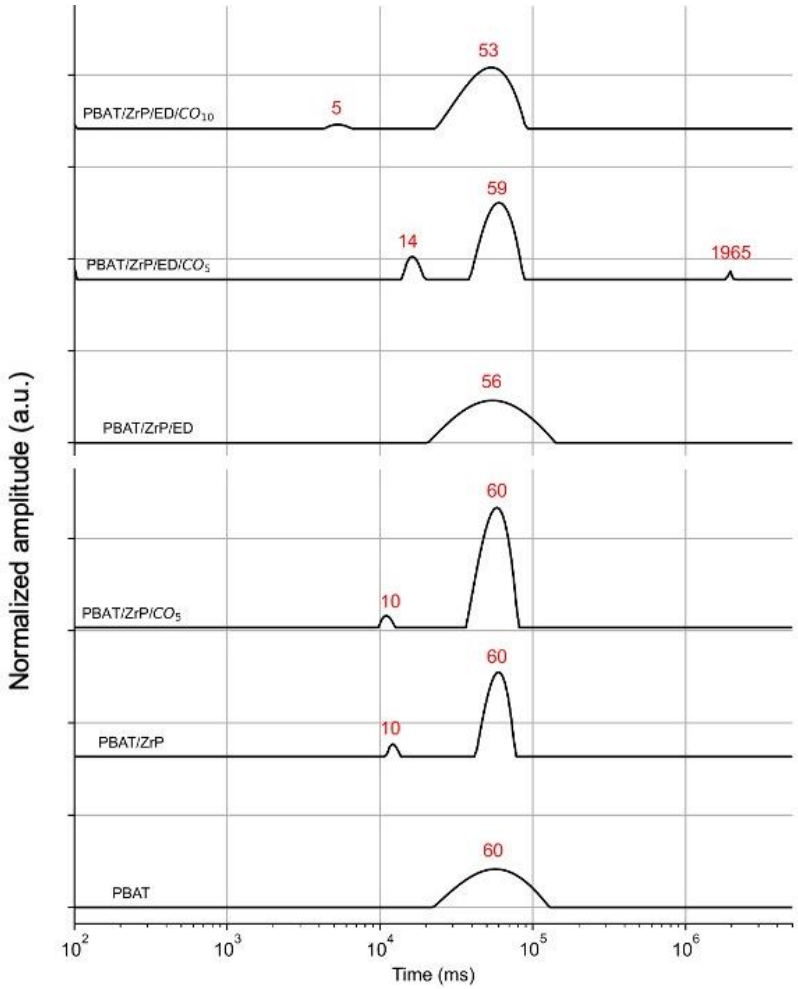

Figure 10: Domain curves expressing the longitudinal relaxation times

ANTIMICROBIAL ACTIVITY

Although bactericidal tests were performed on all samples, only the PBAT/ZrP/ED/CO_{10} composite demonstrated antimicrobial activity. Table 4 shows its inhibitory effects against Gram-positive bacteria, except for L. monocytogenes. The yeast C. albicans, which was also inhibited, exhibited the largest inhibition zone, followed by S. aureus. None of the Gram-negative bacteria tested were inhibited. The lack of inhibition in Gram-negative bacteria suggests that their lipid-rich cell walls hinder the entry of external components, making them more resistant to antimicrobial agents, such as antibiotics and preservatives, compared to Gram-positive bacteria. The result is aligned with data from articles published by Bailey-Hytholt *et al.* and Bril'kov *et al.* [44-45]. A significant pathogen causing foodborne illnesses, *L. monocytogenes* is the Grampositive bacterium that did not exhibit an inhibitory response. This microorganism is known for its resistance to harsh environmental factors, such as acids, salts, sanitizers, and preservatives, compared to other bacterial pathogens [46-47]. A contrasting result was reported by Somrani et al. [48] which observed an inhibition halo of 14.46 mm for *L. monocytogenes*. However, the authors used paper discs impregnated with 95% ethanol-clove oil solution. Shahbazi [49] studied the effects of a clove oil emulsion against L. monocytogenes, *B. cereus, S. aureus*, *Salmonella typhimurium*, and *Escherichia coli*.

Although all Gram-positive and Gram-negative microorganisms were inhibited, the inhibition was significantly lower for four non-pathogenic Gram-positive microorganisms from different *Lactobacillus* species. The recognized antifungal properties of eugenol may explain the stronger inhibition observed against *Candida albicans* [50-51]. Clove oil is a multi-component compound, and its antimicrobial activity can vary depending on the extraction methods used in industrial processing, as well as the experimental methods and conditions employed for testing. Nevertheless, the results indicate that its antimicrobial properties remain effective even after incorporation into the PBAT matrix.

Table 4: Antimicrobial activity data for PBAT/ZrP/ED/CO$_{10}$

Microorganism (ATTC number*)	Zone of inhibition (mm)
Gram negative bacteria	
Escherichia coli 11229	-
Salmonella enteritidis 13076	-
Pseudomonas aeruginosa 15442	-
Gram positive bacteria	
Staphylococcus aureus 29213	6
Bacillus cereus 14579	2
Listeria monocytogenes 19117	-
Yeast	
Candida albicans 10231	12

CONCLUSIONS

In the pursuit of a healthier lifestyle, there is a growing consumer demand for less processed foods. This trend contrasts with the increasing global production of processed foods, which requires ensuring quality and safety while minimizing losses, often through the use of preservatives. In this context, natural compounds, such as clove oil, are gaining attention as potential alternatives. The objective of this work was to combine the biodegradability of PBAT, the nanometric dimensions of ZrP, and the bactericidal properties of clove oil to develop a multifunctional material. Both the phosphate and clove oil components enhanced the hydrophobicity of the films, which is beneficial as it helps to prevent moisture absorption and inhibits microorganism proliferation. Additionally, the incorporation of clove oil further prevents microbial growth. These properties are crucial for packaging films that enhance food safety and extend shelf life. Further studies should explore the antimicrobial activity of the films over time, as well as their combination with other antimicrobial compounds to further improve food microbiological safety and shelf life.

ACKNOWLEDGMENTS

Thanks to Fundação Carlos Chagas Filho de Amparo à Pesquisa do Estado do Rio de Janeiro (FAPERJ) - Processo SEI E-26/200.814/202, Conselho Nacional de Desenvolvimento Cientıfico e Tecnológico (CNPqJ, Fundação Coordenação de Aperfeiçoamento de Pessoal de Nível Superior (CAPES) and Universidade Federal do Rio de Janeiro (UFRJ) to support this research.

Conflicts of Interest

On behalf of all authors, the corresponding author states that there is no conflict of interest.

Data Availability Statement

The datasets generated during and/or analyzed during the current study are not publicly available due to the data are not public (Belong to my Institution – Universidade Federal Rio de Janeiro-UFRJ, Brazil)

References

1. Nagalakshmaiah, M. et al., Biocomposites. Green Composites for Automotive Applications 2019, 197–215.
2. Pinheiro, I. F. et al., Mechanical, Rheological and Degradation Properties of PBAT Nanocomposites Reinforced by Functionalized Cellulose Nanocrystals, European Polymer Journal, 2017, 97, 356–365.
3. Venkatesan, R.; Rajeswari, N. ZnO/PBAT Nanocomposite Films: Investigation on the Mechanical and Biological Activity for Food Packaging, Polymers for Advanced Technologies, 2016, 28 (1), 20–27.
4. Falcão, G. A. et al., PBAT/Organoclay Composite Films: Preparation and Properties, Polymer Bulletin, 2017, 74 (11), 4423–4436.
5. Ferreira, F. V. et al., An Overview on Properties and Applications of Poly (Butylene Adipate-Co-terephthalate)–Pbat Based Composites, Polymer Engineering & Science, 2017, 59(s2).
6. Gülçin, İ. et al., Antioxidant Activity of Clove Oil – a Powerful Antioxidant Source, Arabian Journal of Chemistry, 2012, 5 (4), 489–499.
7. Hu, Q. et al., Progress on the Antimicrobial Activity Research of Clove Oil and Eugenol in the Food Antisepsis Field, Journal of Food Sciences, 2018, 83 (6), 1476–1483.
8. Lu, W. et al., Influence of Clove Essential Oil Immobilized in Mesoporous Silica Nanoparticles on the Functional Properties of Poly (Lactic Acid) Biocomposite Food Packaging Film, Journal of Materials Research and Technology, 2021, 11, 1152–1161.
9. Begum, N. M. et al., In Clove (Syzygium aromaticum) Chemistry, Functionality and Applications, Academic Press, 2022, 203–208.
10. Morelli, C. L. et al., Natural Copaiba Oil as Antibacterial Agent for Bio-Based Active Packaging, Industrial Crops and Products, 2015, 70, 134–141.
11. Santos, T. T. et al., Effect of Filler Type on Properties of PBAT/Organoclay Nanocomposites, Polymer Bulletin, 2019, 77 (2), 901–917.
12. Ferreira, F. V. et al., Silver Nanoparticles Coated with Dodecanethiol Used as Fillers in Non-Cytotoxic and Antifungal PBAT Surface Based on Nanocomposites, Materials Science and Engineering C, 2019, 98, 800–807.
13. Venkatesan, R. et al., Antimicrobial, Mechanical, Barrier, and Thermal Properties of Bio-based Poly (Butylene Adipate-Co-terephthalate) (Pbat)/Ag2o Nanocomposite Films for Packaging Application, Polymers for Advanced Technology, 2017, 29 (1), 61–68.
14. Freitas, D. F. S. et al., Polyamide-6/Organointercalated Lamellar Zirconium Phosphate Nanocomposites: Molecular Mobility, Crystallography and Thermo-Mechanical Evaluation, Journal of Nanoscience and Nanotechnology, 2017, 17 (5), 3042–3050.
15. Freitas, D. F. S. et al., The Role of Octadecylamine as Zirconium Phosphate Intercalating Agent on Poly (Vinyl Alcohol)/Poly(n-Vinyl-2-Pyrrolidone) Biodegradable Systems, Journal of Thermal Analysis and Calorimetry, 2020, 147 (1), 315–325.

16. Mendes, L. C. et al., Zirconium Phosphate Organically Intercalated/Exfoliated with Long Chain Amine, Journal of Thermal Analysis and Calorimetry, 2014, 118 (3), 1461–1469.

17. Xiao, H. et al., Crystallization Behavior of Fully Biodegradable Poly (Lactic Acid)/Poly(Butylene Adipate-Co-terephthalate) Blends, Journal of Applied Polymer Science, 2009, 112 (6), 3754–3763. International Organization for Standardization, Plastics —

18. Thermomechanical analysis (TMA) Part 2: Determination of coefficient of linear thermal expansion and glass transition temperature (ISO Standard No. 11359-2), 2021.

19. Weng, Y.-X. et al., Biodegradation Behavior of Poly (Butylene Adipate-CoTerephthalate) (PBAT), Poly(Lactic Acid) (PLA), and Their Blend under Soil Conditions, Polymer Testing, 2013, 32 (5), 918–926.

20. Zhai, X. et al., Effects of Starch Filling on Physicochemical Properties, Functional Activities, and Release Characteristics of PBAT-Based Biodegradable Active Films Loaded with Tea Polyphenols, International Journal of Biological Macromolecules, 2024, 277, 134505.

21. Zhang, Y. et al., Preparation of Functionalized Zirconium Phosphate and Its Effect on the Flame Retardancy of Silicone Rubber, RSC Advances, 2018, 8 (1), 111–121.

22. Wu, H. et al., Structure and Properties of Starch/α-Zirconium Phosphate Nanocomposite Films, Carbohydrate Polymers, 2009, 77 (2), 358–364.

23. Carvalho, A. L. et al., The Influence of Zinc Gluconate as an Intercalating Agent on the Structural, Thermal, Morphologic, and Molecular Mobility of Lamellar Nanofiller, Colloid and Polymer Science, 2018, 296 (6), 1079–1086.

24. Popovska, O. Characterization of Clove Oil with a FT-IR ATR Spectroscopic Method, Journal of Agricultural, Food and Environmental Sciences, 2023, 77 (2), 64–72.

25. Rojas, J. et al., Lipidic Matrixes Containing Clove Essential Oil: Biological Activity, Microstructural and Textural Studies, Molecules, 2021, 26 (9), 2425.

26. Venkatesan, R. et al., Development and Characterization of Poly (Butylene Adipate-co-terephthalate) (PBAT) Composites with N, P-Doped Carbons for Food Packaging, Carbon Letters, 2023, 33 (6), 1679–1687.

27. Kang, D. et al., Performance and Mechanism of Mg/Fe Layered Double Hydroxides for Fluoride and Arsenate Removal from Aqueous Solution, Chemical Engineering Journal, 2013, 228, 731–740.

28. Jiang, F. et al., Dispersion-Tribological Property Relationship in Mineral Oils Containing 2D Layered α-Zirconium Phosphate Nanoplatelets, Friction, 2019, 8 (4), 695–707.

29. Moustafa, H.; et al., Sustainable Biodegradable Coffee Grounds Filler and Its Effect on the Hydrophobicity, Mechanical and Thermal Properties of Biodegradable PBAT Composites, Journal of Applied Polymer Science, 2016, 134 (8).

30. Albitres, G. A. et al., Nanocellulose: Effect on Thermal, Structural, Molecular Mobility and Rheological Characteristics of Poly (Butylenes Adipate-Co-Butylene Terephthalate) Nanocomposites, Materials Science and Applications, 2022, 13 (04), 249–277.

31. Li, H., et al., Effect of Titanate Coupling Agent on Antioxidant Property and UV Blocking Property of PBAT/Lignin Composite Films, Polymer Testing, 2024, 140, 108613.

32. Chen, W. et al., The Degradation Investigation of Biodegradable PLA/PBAT Blend: Thermal Stability, Mechanical Properties and Pals Analysis, Radiation Physics and Chemistry, 2021, 180, 109239.

33. González Seligra, P. et al., Influence of Incorporation of Starch Nanoparticles in PBAT/TPS Composite Films, Polymer International, 2016, 65 (8), 938–945.

34. de Matos Costa, A. R. et al., Properties of Biodegradable Films Based on Poly (Butylene Succinate) (PBS) and Poly (Butylene Adipate-Co-Terephthalate) (PBAT) Blends, Polymers, 2020, 12 (10), 2317.

35. Li, X. et al, Effect of Surface Property of Halloysite on the Crystallization Behavior of PBAT, Applied Clay Science, 2018, 157, 218–226.

36. da Silva, C. G. et al., Thermal Stability of the PBAT Biofilms with Cellulose Nanostructures/Essential Oils for Active Packaging, Journal of Thermal Analysis and Calorimetry, 2019, 138 (4), 2375–2386.

37. Tavares, L. B. et al., PBAT/Kraft Lignin Blend in Flexible Laminated Food Packaging: Peeling Resistance and Thermal Degradability, Polymer Testing, 2018, 67, 169–176.

38. Thiyagu, T. T. et al., Effect of Sio2/Tio2 and Zno Nanoparticle on Cardanol Oil Compatibilized PLA/PBAT Biocomposite Packaging Film, Silicon, 2022, 14 (7), 3795–3808.

39. Laorenza, Y.; Harnkarnsujarit, N. Ginger Oil and Lime Peel Oil Loaded PBAT/PLA via Cast-Extrusion as Shrimp Active Packaging: Microbial and Melanosis Inhibition, Food Packaging and Shelf Life, 2023, 38, 101116.

40. Boro, U. et al., Synthesis and Characterization of Poly (Lactic Acid)/Clove Essential Oil/Alkali-Treated Halloysite Nanotubes Composite Films for Food Packaging Applications, International Journal of Biological Macromolecules, 2022, 216, 927–939.

41. Hassan, M., et al., Additive Manufacturing of a Super Toughened Biodegradable Polymer Blend: Structure–Property-Processing Correlation and 3D Printed Prosthetic Part Development, ACS Applied Polymer Materials, 2024, 6 (7), 3849–3863.

42. Josselin, M. et al., Hygro-Thermal Coupling on 4D-Printed Biocomposites as Key for Meteosensitive Shape-Changing Materials, Virtual and Physical Prototyping, 2024, 19(1).

43. Da Rocha, L. V. et al., Thermostructural Evaluation of Poly (Butylene AdipateCo-Terephthalate) /Molybdenum Trioxide Nanocomposites through Time Domain Nuclear Magnetic Resonance and Other Conventional Techniques, Brazilian Journal of Development, 2022, 8 (5), 36588–36601.

44. Bailey-Hytholt, C. M., et al., Assembly of Cell Mimicking Supported and Suspended Lipid Bilayer Models for the Study of Molecular Interactions, Journal of Visualized Experiments, 2021, 174.

45. Bril'kov, M. S. et al., Bacterial Extracellular Vesicles: Towards Realistic Models for Bacterial Membranes in Molecular Interaction Studies by Surface Plasmon Resonance, Frontiers in Molecular Biosciences, 2023, 10.

46. Patra, J. K.; Baek, K.-H, Anti-Listerial Activity of Four Seaweed Essential Oils against Listeria Monocytogenes, Jundishapur Journal of Microbiology 2016, 9 (7).

47. Hu, M. et al, A Meta-Analysis and Systematic Review of Listeria Monocytogenes Response to Sanitizer Treatments, Foods, 2022, 12 (1), 154.

48. Somrani, M., et al, Antibacterial and Antibiofilm Activity of Essential Oil of Clove against Listeria Monocytogenes and Salmonella Enteritidis, Food Science and Technology International, 2021, 28 (4), 331–339.

49. Shahbazi, Y., Antioxidant, antibacterial, and antifungal properties of nanoemulsion of clove essential oil, Nanomedicine Research Journal, 2019, 4(4), 204-208.

50. Shahina, Z., et al., Cinnamon Leaf and Clove Essential Oils Are Potent Inhibitors of Candida Albicans Virulence Traits, Microorganisms, 2022, 10 (10), 1989.

51. Yassin, M. T., et al., In Vitro Anticandidal Potency of Syzygium Aromaticum (Clove) Extracts against Vaginal Candidiasis, BMC Complementary Medicine and Therapies, 2020, 20 (1).